Eur J Nucl Med Mol Imaging (2008) 35:174–185
DOI 10.1007/s00259-007-0553-8

ORIGINAL ARTICLE

Are [*O-methyl*-^{11}C]derivatives of ICI 89,406 β_1-adrenoceptor selective radioligands suitable for PET?

Marilyn P. Law · Stefan Wagner · Klaus Kopka · Victor W. Pike · Otmar Schober · Michael Schäfers

Received: 23 February 2007 / Accepted: 15 July 2007 / Published online: 29 September 2007

Abstract
Purpose Radioligand binding studies show that β_1-adrenoceptor (β_1-AR) density may be reduced in heart disease without down regulation of β_2-ARs. Radioligands are available for measuring total β-AR density non-invasively with clinical positron emission tomography (PET) but none are selective for β_1- or β_2-ARs. The aim was to evaluate ICI 89,406, a β_1-AR-selective antagonist amenable to labelling with positron emitters, for PET.
Methods The *S*-enantiomer of an [O-*methyl*-^{11}C] derivative of ICI 89,406 ((*S*)-[^{11}C]ICI-OMe) was synthesised. Tissue radioactivity after *i.v.* injection of (*S*)-[^{11}C]ICI-OMe (< 2 nmol·kg^{-1}) into adult Wistar rats was assessed by small animal PET and post mortem dissection. Metabolism was assessed by HPLC of extracts prepared from plasma and tissues and by measuring [^{11}C]CO_2 in exhaled air.
Results The heart was visualised by PET after injection of (*S*)-[^{11}C]ICI-OMe but neither unlabelled (*S*)-ICI-OMe nor propranolol (non-selective β-AR antagonist) injected 15 min after (*S*)-[^{11}C]ICI-OMe affected myocardial radioactivity. Ex vivo dissection showed that injecting unlabelled (*S*)-ICI-OMe, propranolol or CGP 20712A (β_1-selective AR antagonist) at high dose (> 2 μmol·kg^{-1}) before (*S*)-[^{11}C]ICI-OMe had a small effect on myocardial radioactivity. HPLC demonstrated that radioactivity in myocardium was due to unmetabolised (*S*)-[^{11}C]ICI-OMe although ^{11}C-labelled metabolites rapidly appeared in plasma and liver and [^{11}C]CO_2 was detected in exhaled air.
Conclusion Myocardial uptake of (*S*)-[^{11}C]ICI-OMe after *i.v.* injection was low, possibly due to rapid metabolism in other tissues. Injection of unlabelled ligand or β-AR antagonists had little effect indicating that binding was mainly to non-specific myocardial sites, thus precluding the use of (*S*)-[^{11}C]ICI-OMe to assess β_1-ARs with PET.

Keywords ICI 89,406 derivative · β_1-adrenoceptor-selective radioligand · PET radioligand · Myocardial β_1-adrenoceptors · Small animal PET

M. P. Law (✉) · S. Wagner · K. Kopka · O. Schober · M. Schäfers
Department of Nuclear Medicine, University Hospital Münster,
Albert-Schweitzer-Str. 33,
48149 Münster, Germany
e-mail: mplaw@uni-muenster.de

V. W. Pike
Molecular Imaging Branch, National Institute of Mental Health,
National Institutes of Health,
10 Center Drive, Rm B3 C346A, MSC 1003,
Bethesda, MD 20892-1003, USA

Introduction

In the normal heart, β-adrenoceptors (β-AR) play the major role in adrenergic control of myocardial function. Three β-AR subtypes have been identified in mammals [1, 2]. The β_1 and β_2 subtypes are responsible for the positive chronotropic and inotropic effects of the catecholamines noradrenaline and adrenaline. Both are cell surface receptors that couple to the stimulatory G_s-protein thereby activating adenylyl cyclase. β_2-AR agonists, such as salbutamol, may activate the inhibitory G_i-protein pathway which reduces contraction [1, 2]. The β_3-ARs may also have a cardiac depressant effect via the nitric oxide pathway. There is evidence in mice and rats that β_1-AR can also promote apoptosis of myocytes mediated by increases in intravellular Ca^{2+} which stimulate Ca^{2+}-calmodulin-dependent protein kinase II, whereas β_2-AR coupling to G_i-protein may inhibit apoptosis [1, 2].

There are two major lines of evidence that suggest that β-ARs play a major role in heart failure [1–3]. First, overactivation of sympathetic nerves leads to an increased spillover of noradrenaline from the heart to the plasma, a phenomenon which is predictive of cardiac death [1, 3]. Second, cardiac β-AR density is decreased and downstream mechanisms are altered [1–3]. Although an increase in adrenergic drive may maintain cardiac output in the early stages of disease, continued stimulation may be detrimental and contribute to heart failure. Clinically, β-AR antagonists were first used in patients with heart failure to reduce the tachycardia that was considered to be detrimental. Subsequent clinical trials of metoprolol, carvedilol and bisoprolol demonstrated reduced morbidity and mortality and consequently the use of β-AR antagonists is now standard treatment of heart failure [1, 3].

In many studies there is a preferential downregulation of β_1-AR density [5–8] but decreases in both β_1 and β_2-AR density have been reported [5–7, 9]. Although clinically β-AR antagonists have become established in the management of heart failure, it is not clear whether or not there is an advantage in selectively blocking β_1-ARs [1, 3]. Furthermore, there is growing evidence that both β_1- and β_2-AR genes have genetic polymorphisms [10]. Although it seems that these polymorphisms do not play a role as disease-causing genes they may be risk factors and may influence disease progression and responses to therapeutic drugs [10]. A better understanding of the changes in each β-AR subtype in the various types of cardiac disease may lead to may lead to therapeutic approaches more taylored to the individual patient.

Positron emission tomography (PET) with appropriate radioligands may be used to measure β-AR density non-invasively in humans or in animal models of human disease. Radioligands, for example (*S*)-[^{11}C]CGP 12177 [11–15] and [^{11}C]CGP 12388 [16, 17], are available for quantifying total β-AR density in a clinical setting but none is suitable for assessing β_1- or β_2-subtypes using PET. Subtype β_1-AR selective radioligands have been synthesised for PET, for example (+/−)-[^{11}C]HX-CH 44 [18], (*S*)-[^{11}C]bisoprolol [19] or [^{11}C]CGP 20712A [20] and its *S*-enantiomer [^{11}C]CGP 26505 [21]. None of these radioligands, however, is appropriate for use in PET because of high non-specific binding, rapid metabolism or tissue uptake that does not reflect binding to β_1-ARs [18–20].

ICI 89,406 (Fig. 1) is a β_1-AR-selective antagonist. Although membrane binding studies show that the *S*-enantiomer is more potent than the *R*-enantiomer, the racemate produces effective β_1-AR blockade during exercise in patients with angina pectoris [22–24]. Considering the efficacy and β_1-selectivity of the racemate, we chose this compound as a lead structure for the development of new β_1-AR-selective ligands for single photon emission computed tomography (SPECT) and PET. To examine the structure activity relationships (SARs) between potential ligands and β-ARs, the aromatic substituents and lengths of the aliphatic chains were modified giving 20 derivatives. Competition studies using the non-selective AR radioligand [^{125}I]iodocyanopindolol ([^{125}I]ICYP) and murine myocardial membranes showed that 16 derivatives were selective for β_1-ARs (high affinity inhibition constant K_{i1}, 0.02–35 nM; low affinity inhibition constant K_{i2}, 12–16000 nM; β_1-selectivity K_{i1}/K_{i2}, 12–16,000 [25]. Of these, two iodinated derivatives I-ICI-H [26] and I-ICI-COOH [27] showed high affinity and selectivity in vitro but neither the radiolabelled compound [$^{123/125}$I]I-ICI-H nor [$^{123/125}$I]I-ICI-COOH was suitable for in vivo studies due to high non-specific binding [26] or rapid de-iodination [27].

A third derivative showing high affinity and selectivity was amenable to labelling with carbon-11. Recently we described the synthesis and in vitro assessment of both enantiomers of this compound, namely (*R*)- and (*S*)-*N*-[2-[3-(2-cyano-phenoxy)-2-hydroxy-propylamino]-ethyl]-*N*′-(4-methoxy-phenyl)-urea (Fig. 1) [28]. Membrane studies showed that both enantiomers exibited high affinity and selectivity for β_1-ARs (Fig. 1). Therefore, each was labelled with carbon-11 in the *O-methyl* position to give (*R*)-[^{11}C]ICI-OMe and (*S*)-[^{11}C]ICI-OMe (Fig. 1) [28].

The development of small animal scanners offers the possibility of preclinical assessment of potential ligands using fewer animals than are required using ex vivo dissection techniques. The quadHIDAC small animal PET scanner [29] has especially good spatial resolution and high sensitivity [30, 31]. Preliminary studies in mice, using HIDAC scanning, demonstrated myocardial uptake of radioactivity after intravenous injection of (*S*)-[^{11}C]ICI-OMe [32] (Fig. 2). This uptake, however, was not blocked by pre-dosing with unlabelled (*S*)-ICI-OMe (data not shown) or propranolol (Fig. 2).

For tracer kinetics to hold, the amount of radioligand used in in vivo scanning must give low receptor occupancy (e.g. 1%). At such levels competition with endogenous compounds should not exclude visualisation of the receptor of interest. Although dedicated small animal scanners provide high spacial resolution and sesnsitivity, the specific radioactivity achievable for a given radioligand may preclude the attainment of such low occupancies [33]. The doses of [^{11}C]ICI-OMe required in mice to give an amount of radioactivity detectable by in vivo scanning (Fig. 2) were equivalent to > 20 nmol·(kg mouse body weight)$^{-1}$. This dose may be sufficient to saturate myocardial β_1-ARs resulting in a non-specific PET signal. This is exemplified by studies of the non-selective β-AR ligand (*S*)-[^{11}C]CGP 12177 in rats. Ex vivo, the dose of (*S*)-CGP 12177 required to saturate half the β-ARs in the left ventricle wall was 1.3 nmol·kg^{-1} and a dose of 15 nmol·kg^{-1}

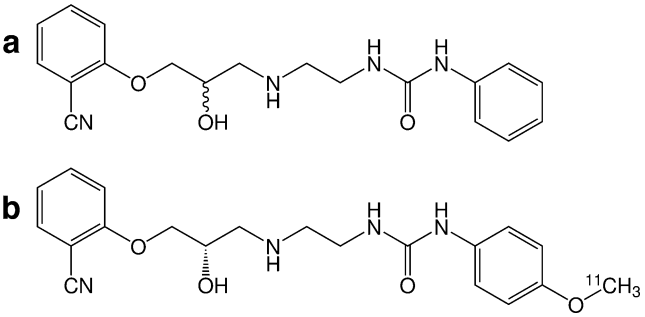

Fig. 1 Structure of the β_1-adrenoceptor antagonist ICI 89,406 (**a**) and its derivative *N*-[2-[3-(2-cyano-phenoxy)-2-hydroxy-propylamino]-ethyl]-*N'*-(4-methoxy-phenyl)-urea (ICI-OMe) (**b**). The binding characteristics of (*R*)- and (*S*)-ICI-OMe to β_1- and β_2-adrenoceptors were assessed by competition studies using murine myocardial membranes and [^{125}I]ICYP [28]. *R*-isomer: K_{i1}=0.29±0.03 nM, K_{i2}=1760±300 nM, β_1-selectivity=6100±1540; *S*-isomer: K_{i1}=0.07±0.02 nM, K_{i2}=83±33 nM, β_1-selectivity=1240±280)

completely blocked myocardial uptake of radioactivity [34]. In vitro membrane binding studies show that the K_D for CGP 12177 is between 0.19 and 0.67 nM for rat myocardium [35–39], i.e. numerically 2 to 10 times lower than the ex vivo half saturation dose. If there were a similar relationship between in vitro K_i and ex vivo half saturation dose for (*S*)-ICI-OMe (K_{i1} 0.07 nM [28]) an ex vivo half saturation dose of 0.14 nmol·kg^{-1} might be expected, in which case the dose of 20 nmol·kg^{-1} used for HIDAC scanning of mice would completely saturate myocardial β-ARs.

It may possible to inject sufficient radioactivity for PET scanning without saturating myocardial β-ARs in the rat even if myocardial β-AR receptor density is the same as in the mouse [33]. β-AR receptor density in the rat, however, may be higher. There are many reported estimates of B_{max} for rat myocardial membranes, giving values in the range 12–70 fmol/mg protein [34–39]. There are fewer estimates for mouse but two recent papers give values in the lower range (11–16 fmol/mg protein) [40, 41].

Another advantage of the rat is that metabolism of ICI-OMe may be less rapid than in the mouse. A possible pathway for metabolism of (*S*)-[^{11}C]ICI-OMe is cleavage of the molecule by methyl transferases to give [^{11}C]methanol. Methanol is converted into formaldehyde, principally in the liver, by alcohol dehydrogenase. Formaldehyde is then converted by aldehyde dehydrogenase into formate [42] which is oxidised to carbon dioxide by a folate-dependent one-carbon pool pathway [43–45].

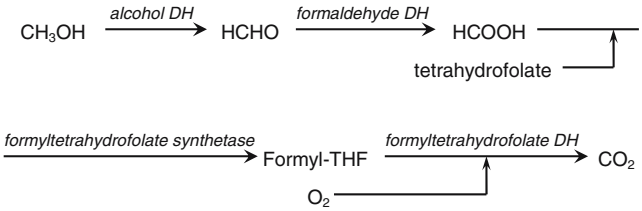

The rate of oxidation is regulated by hepatic concentrations of tetrahydrofolate [46]. One study has shown that the rate of formate oxidation, assayed in liver homogenates, is four times higher in mice than in rats (300 *v* 75 mg·kg^{-1}·h^{-1}) [47].

The present paper describes the evaluation of (*S*)-[^{11}C]ICI-OMe in the rat. Myocardial uptake was assessed using the quadHIDAC scanner and specificity for β-ARs was tested by injection of unlabelled ICI-OMe or propranolol. Ex vivo dissection studies, using lower doses of (*S*)-[^{11}C]ICI-OMe, were carried out for comparison. If (*S*)-[^{11}C]ICI-OMe were to be metabolised by methanol and formate radioactive carbon dioxide would be detectable. Therefore, radioactivity in exhaled air was assessed in addition to the usual HPLC assessment of radiolabelled metabolites in plasma and tissues.

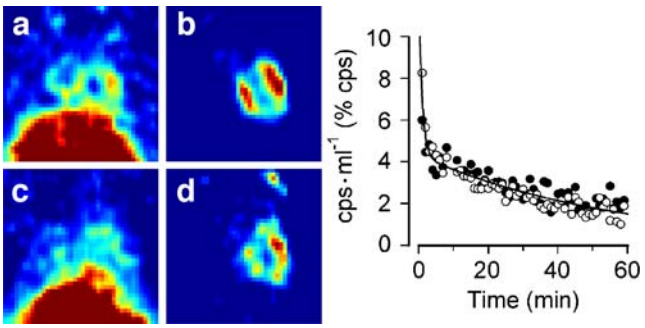

Fig. 2 Uptake of radioactivity after intravenous injection of (*S*)-[^{11}C]ICI-OMe into mice, visualised using the quadHIDAC PET scanner. Male CD1 mice (25–30 g) were anaesthetised by inhalation (isoflurane 2%, oxygen 0.5 l·min^{-1}) for insertion of catheters into tail veins and subsequent PET scanning. Two mice were positioned in the scanner and 30 s after scan start (*S*)-[^{11}C]ICI-OMe (4 MBq in 100 μl) was injected into each mouse simultaneously. List mode data were reconstructed into a 10 min frame (5–15 min scan time) and sub-images of the hearts made (panels **a**, **c**). Injection of [^{18}F]FDG (4 MBq) after the (*S*)-[^{11}C]ICI-OMe scan confirmed the position of the heart (panels **b**, **d**). Myocardial uptake, assessed by drawing regions of interest in myocardium identified by the corresponding [^{18}F]FDG scan (8 planes), was expressed as a percentage of the total radioactivity in a cube drawn round each mouse and plotted against mid-frame time after injection (graph). Mouse 1 received (*S*)-[^{11}C]ICI-OMe alone (panel **a**, **b**; •) and mouse 2 propranolol (15 μmol·kg^{-1}) 5 min before (*S*)-[^{11}C]ICI-OMe (panels **c**, **d**; ○). Although the heart was visualised after injecting (*S*)-[^{11}C]ICI-OMe (panel **a**, •), myocardial uptake was not reduced by predosing with unlabelled (*S*)-ICI-OMe (panel **c**, ○)

Methods

Radiochemistry

(*S*)-ICI-OMe ((*S*)-[*O-methyl*-^{11}C]-*N*-[2-[3-(2-cyano-phenoxy)-2-hydroxy-propylamino]-ethyl]-*N'*-(4-methoxy-phenyl)-urea)

was synthesised from its desmethyl precursor, (*S*)-*N*-[2-[3-(2-cyano-phenoxy)-2-hydroxy-propylamino]-ethyl]-*N'*-(4-hydroxy-phenyl)-urea by radioalkylation with [^{11}C] iodomethane. Details of the radiosynthesis are given elsewhere [28]. Radioactivities of products ranged from 1.2 to 2.7 GBq at the end of synthesis (EOS), the radiochemical yield being 44.1±5.0% after 41.2±3.4 min synthesis time (n=14) from the end of radionuclide production (EOB). As determined by analytical radio-HPLC, radiochemical purities of 97.4±1.3% and specific activities of 26.4±9.4 GBq·μmol^{-1} at EOB were achieved (n=14).

Pharmaceuticals

Unlabelled (*S*)-ICI-OMe was prepared as described previously [28]. It was dissolved in ethanol/saline (1/1, v/v) at 2 μmol·ml^{-1} for injection into animals.

The non-selective β-AR antagonists propranolol·HCl and CGP 12177·HCl and the β_1-AR selective antagonist CGP 20712A were purchased from Sigma Aldrich Chemie GmbH (Germany). These antagonists were dissolved in saline at concentrations of 100 nmol·ml^{-1} or 5 μmol·ml^{-1} for injection.

Animals

Studies were approved by the Federal Animal Rights Committee and were performed in accordance with institutional guidelines for health and care of experimental animals.

Male Wistar rats (280–300 g) were anaesthetised by inhalation (isoflurane 2%, oxygen 0.5 l·min^{-1}) for insertion of indwelling catheters into the ventral tail artery and one lateral tail vein. Animals were allowed to recover for 1–2 h under light restraint (Bollman's cages) before being re-anaesthetised for PET scanning. Ex vivo biodistribution studies were carried out in conscious animals [34].

PET scanning

PET was carried out using a sub-millimeter high resolution (0.7 mm full width at half maximum) dedicated small animal scanner (32 module quadHIDAC, Oxford Positron Systems Ltd., UK) which uses wire-chamber detectors and offers uniform spatial resolution (< 1 mm) over a large cylindrical field (165 mm diameter, 280 mm axial length) [29–31].

Two anaesthetized rats (isoflurane 2%, oxygen 0.5 l·min^{-1} per rat) were placed on a heating pad to maintain body temperature during the scan. Animals were positioned on the scanner and 30 s after the start of data acquisition (*S*)-ICI-OMe (8–11 MBq in 200 μl per rat; 1–5 nmol·kg^{-1}) was injected simultaneously into each rat via the tail vein catheters. For each scan, one rat was given unlabelled (*S*)-ICI-OMe (2 μmol·kg^{-1}) or the non-selective β-AR blocker propranolol (5 μmol·kg^{-1}) 5 min before or 15 min after injection of (*S*)-[^{11}C]ICI-OMe. To confirm the location of the heart, [^{18}F]2-fluoro-2-deoxy-D-glucose ([^{18}F]FDG) (8 MBq in 200 μl per rat) was injected via the tail vein 5–10 min after completion of the (*S*)-[^{11}C]ICI-OMe scan and data were acquired for 30 min. To improve myocardial uptake of [^{18}F]FDG, 0.5 mL glucose (20%) was injected 5 min before [^{18}F]FDG.

List-mode data were acquired for 60 min ((*S*)-[^{11}C]ICI-OMe) or 30 min ([^{18}F]FDG) and subsequently reconstructed into an image volume of 160×160×280 mm (voxel size 0.4×0.4×0.4 mm) in time frames of 1 or 10 min for (*S*)-[^{11}C]ICI-OMe and 15 min for [^{18}F]FDG, using an iterative reconstruction algorithm [48]. PET images were analysed using in-house software programmes in MATLAB (The MathWorks Company) and C programming languages [30, 49].

To assess the total radioactivity in each animal, a cube encompassing the body, excluding the tail and paws, was drawn on the reconstructed [^{18}F]FDG image (15–30 min time frame). The parameters defining this cube were saved and used to compute the whole body radioactivities for each time frame of the (*S*)-[^{11}C]ICI-OMe scan.

The parameters required to create images of each heart and compute time-activity curves were also defined using the [^{18}F]FDG scan (15–30 min time frame). The reconstructed volume was divided into two and each resulting sub-image was rotated (rat head first in scanner) or flipped (rat tail first in scanner) so that each rat was visualised as in clinical practice, i.e. lying on its back, head in scanner. From the sub-images, coronal images (120×120×120 pixels) encompassing the heart were made. Myocardial regions of interest (left ventricle wall and septum) were traced manually on these images. The parameters were saved and used to create heart images (time frames 5–15 min and 20–30 min) and decay-corrected time-activity curves (cps·ml^{-1} *vs* mid-frame time, for each 1 min-time frame after injection) for the (*S*)-[^{11}C]ICI-OMe scan.

Ex vivo biodistribution studies

(*S*)-[^{11}C]ICI-OMe or unlabelled antagonists were injected as a bolus (100 nmol·kg^{-1}-5 μmol·g^{-1}, 1 μl·g^{-1} body weight) via the tail vein. Aliquots of each (*S*)-[^{11}C]ICI-OMe injectate were diluted in ethanol/saline and measured to determine the radioactivity injected into each rat. Six sequential arterial blood samples (ca. 100 μL) were taken from some rats. An aliquot of whole blood was taken and the remainder centrifuged to separate the plasma. Rats were sacrificed by intravenous injection of sodium pentobarbitone (Euthatal®)

at 200 mg·(kg body weight)$^{-1}$ at predetermined times after injection. Blood was taken by cardiac puncture and tissues rapidly removed. Tissue samples were blotted dry using filter paper and transferred to weighed vials for reweighing and measurement of radioactivity using an automated gamma counter (Wallac Wizard 3″, Perkin Elmer Life Sciences, Boston, USA). Radioactivity was expressed as cpm·(g wet tissue)$^{-1}$.

In a preliminary experiment, using four rats, there was a linear relationship between myocardial uptake, expressed as cpm·(g wet tissue)$^{-1}$, and injected radioactivity between doses of 0.4 to 18 MBq·kg^{-1}, equivalent to 0.35 to 1.4 nmol·kg^{-1}. Therefore, to correct for differences in animal body weight and injected dose, results were expressed as an uptake index, defined as:

$$\text{Uptake index} = \frac{\text{Tissue radioactivity (cpm)}/\text{Tissue wet weight (g)}}{\text{Radioactivity injected (cpm)}/\text{Body weight (g)}}$$

HPLC analysis of radiolabelled metabolites

Radioactive metabolites in plasma, myocardium, liver and urine were assessed by gradient RP-HPLC. Rats (250–320 g) were anaesthetised for insertion of catheters into the ventral tail artery and one lateral tail vein and were allowed to recover from the anaesthesia for ~2 h before injection of 60–150 MBq (20–40 nmol·kg^{-1}) (*S*)-[^{11}C]ICI-OMe via the tail vein catheters. Up to three blood samples (1 ml) were collected from the tail artery catheter at 2 to 25 min after injection of radioligand. Cell free plasma was prepared by centrifuging each blood sample at 2000 g for 2 min. Ice-cold acetonitrile (0.7 ml) was added to the plasma (0.5 ml) and the precipitated proteins were removed by centrifugation. A sample of the resulting supernatant (200 μl) was spiked with non-radioactive (*S*)-ICI-OMe (10 μg) and analysed.

Rats were killed at 2, 5 and 15 min after injection of (*S*)-[^{11}C]ICI-OMe and samples of heart (left and right ventricular walls and septum) and liver were transferred to 3 ml ice-cold acetonitrile. Tissues were minced with scissors, transferred to a tube and the volume made up to 6 ml before homogenising using a Polytron rotor homogeniser at half maximum speed for 2 min. The homogenate was centrifuged at 2000 g for 5 min. The supernatant was evaporated to dryness and the residue taken up into 500 μl eluent B (see below). If cloudy, the resulting solution was centrifuged and 200 μl of the supernatant, spiked with non-radioactive (*S*)-ICI-OMe (10 μg), were analysed. Urine samples (200 μl) were spiked with non-radioactive (*S*)-ICI-OMe (10 μg) and injected onto the HPLC system.

The gradient RP-HPLC-chromatograph system comprised a Nucleosil 100 C-18 column (5 μ; 250×4.6 mm) with a corresponding precolumn (20×4.0 mm) eluted at 2 ml/min with a mixture of eluent A (MeCN /H_2O/TFA; 950/50/1 by vol.) and eluent B (MeCN/H_2O/TFA; 50/950/1 by vol.) according to the programme eluent B from 92% to 50% within 15 min, 10 min halt and then from 50% to 92% within 5 min. Eluate was monitored for radioactivity and absorbance at 254 nm.

The percentages of (*S*)-[^{11}C]ICI-OMe and its radioactive metabolites were calculated by integration of the HPLC radiochromatogram after correction for background and radioactive decay.

Exhaled [^{11}C]CO_2

To measure exhaled [^{11}C]CO_2, rats were anaesthetised by intraperitoneal injection of ketamine (90 mg·kg^{-1})/midazolam (10 mg·kg^{-1}). A mask was placed over the head and exhaled air drawn through sodium hydroxide traps (trap position 1, 8 ml 1 M NaOH in 10 ml vial; trap position 2, 70 ml 1 M NaOH in 100 ml vial) using a vacuum pump. (*S*)-[^{11}C]ICI-OMe (10 MBq) was injected via a tail vein catheter and the trap in position 1 was replaced manually by a new trap (8 ml 1 M NaOH) using a predetermined time sequence (5×1 min, 3×5 min, 4×10 min, 3×20 min). Radioactivity in the 10 ml vials was measured using the automated gamma counter (Wallac Wizard 3″) during the course of the study. Radioactivity in each vial was expressed as a rate given by:

$$\text{cpm/min (\%)} = 100 * \frac{\text{Radioactivity in vial (cpm)}/\text{collection time (min)}}{\text{Radioactivity injected (cpm)}}$$

Radioactivity in samples taken from the second trap (100 mL vial) was measured at the end of the measurement period (60 min) to assess the proportion of exhaled [^{11}C]CO_2 not trapped in the 10 mL vials.

[^{11}C]CO_2 in plasma

[^{11}C]CO_2 in blood was measured essentially as described by Gunn et al. [50]. (*S*)-[^{11}C]ICI-OMe (10 MBq) was injected via a tail vein catheter into rats and blood samples taken from a tail artery catheter at predetermined times after injection. At each time, blood (50 μl) was added to 0.5 M NaOH (200 μl) and the tube capped (A). Blood (50 μl) was added to isopropanol (150 μl) to which was added 0.5 M HCl (50 μl). This solution was sonicated in warm water to release [^{11}C]CO_2 (B). Radioactivity was measured. The percentage of plasma radioactivity due to [^{11}C]CO_2 is given by:

$$\text{Plasma } [^{11}\text{C}]CO_2(\%) = 100 * (\text{cpm}_A - \text{cpm}_B)/\text{cpm}_A$$

Results

PET scanning of rats

Figure 3 illustrates the biodistribution of radioactivity after intravenous injection of (*S*)-[^{11}C]ICI-OMe. Two rats were placed on their fronts in the quadHIDAC scanner and (*S*)-[^{11}C]ICI-OMe was injected simultaneously into each. The reconstructed images were rotated in the sagittal plane so that coronal images show the rats lying on their backs, rat 1 tail in scanner with its heart to the left of the image and rat 2 head in scanner with its heart to the right. Data for thirteen planes were summed to show the heart chambers. The heart can be seen but there was high uptake of radioactivity in liver, intestine, kidney and bladder (Fig. 3, panel a). The heart was still visible after the injection of unlabelled ICI-OMe (Fig. 3, panel b). The position of the heart was confirmed by the [^{18}F]FDG scan carried out after completion of the (*S*)-[^{11}C]ICI-OMe scan (Fig. 3, panel c).

Figure 4 shows coronal images of the thoraces of the rats shown in Fig. 3. Data for thirteen planes were summed to give the images shown in panels a to f. Unlabelled (*S*)-ICI-OMe injected 15 min after (*S*)-[^{11}C]ICI-OMe had no obvious effect on the later images (Fig. 4, panel e). One minute time frames were reconstucted for the (*S*)-[^{11}C]ICI-OMe scan and time-activity curves were computed for regions of interest drawn round the left ventricle wall and septum (13 planes). Myocardial radioactivity was detected immediately after injection and reached a maximum during the first minute. The early phase (< 5 min) of rapid loss from the left ventricle wall and septum was followed by a slow loss of myocardial radioactivity. Injection of unlabelled (*S*)-ICI-OMe had no significant effect on this loss. The whole body cps for the two rats were comparable but showed a small increase (7%) during the (*S*)-[^{11}C]ICI-OMe scan, presumably an artefact of the reconstruction algorithm.

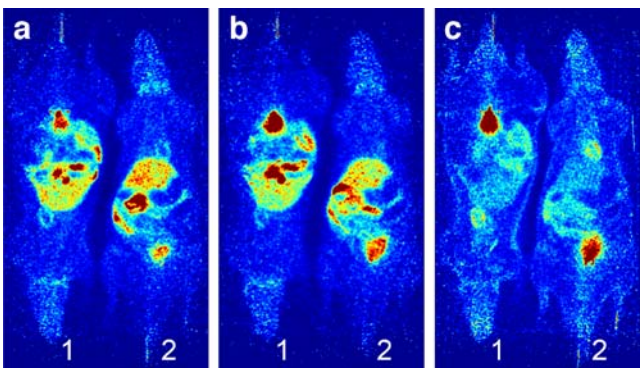

Fig. 3 Distribution of radioactivity in rats after intravenous injection of (*S*)-[^{11}C]ICI-OMe visualised by the quadHIDAC scanner. Two rats were placed in the scanner and (*S*)-[^{11}C]ICI-OMe (8 MBq per rat in 200 μl, 1 nmol·kg^{-1}) was injected simultaneously into each. 15 min after (*S*)-[^{11}C]ICI-OMe, rat 1 received vehicle (200 μl: ethanol/saline, 1/1, v/v) and rat 2 unlabelled (*S*)-ICI-OMe (2 μmol·kg^{-1}, 200 μl). Both rats received [^{18}F]FDG (8 MBq per rat in 200 μl) after the (*S*)-[^{11}C]ICI-OMe scan. The images show the rats lying on their backs, rat 1 tail in scanner with its heart to the left of the image, rat 2 head in scanner with its heart to the right. Data for thirteen planes were summed to show the heart chambers. Panel **a**: 5–15 min after injection of (*S*)-[^{11}C]ICI-OMe. Panel **b**: 20–30 min after (*S*)-[^{11}C]ICI-OMe, i.e. 5–10 min after vehicle (rat 1) or unlabelled (*S*)-ICI-OMe (rat 2). Panel **c**: 15–30 min after [^{18}F]FDG

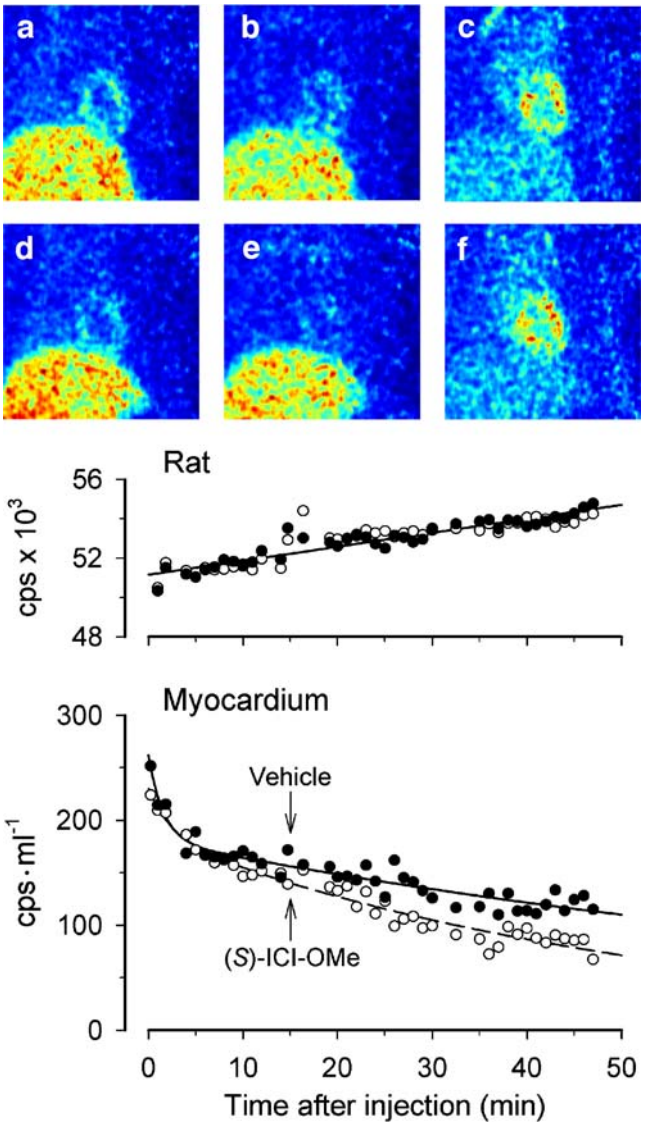

Fig. 4 Uptake of radioactivity in the rat heart after intravenous injection of (*S*)-[^{11}C]ICI-OMe visualised by the quadHIDAC PET scanner. Two rats were placed in the scanner (rat 1: panels **a**–**c**; rat 2 panels **d**–**e**). (*S*)-[^{11}C]ICI-OMe (8 MBq per rat in 200 μl, 1 nmol·kg^{-1}) was injected simultaneously into each and the heart was visualised by summing thirteen myocardial planes at 5–15 min (panels **a**, **d**). 15 min after (*S*)-[^{11}C]ICI-OMe, rat 1 received vehicle (200 μl: ethanol/saline, 1/1, v/v) and rat 2 unlabelled (*S*)-ICI-OMe (2 μmol·kg^{-1}, 200 μl). Myocardial images at 20–30 min were comparable (panels **b**, **e**). Both rats received [^{18}F]FDG (8 MBq per rat in 200 μl) after the (*S*)-[^{11}C]ICI-OMe scan (panels **c**, **f**). Time activity curves were computed (*S*)-[^{11}C]ICI-OMe (see text). ● vehicle; ○ unlabelled (*S*)-ICI-OMe

Similar results were obtained when propranolol (10 μmol·kg^{-1}), which blocks β-AR in vivo in rats (34), was injected after (*S*)-[^{11}C]ICI-OMe and predosing rats by injecting unlabelled (*S*)-ICI-OMe (2 μmol·kg^{-1}) had no effect on myocardial uptake of (*S*)-[^{11}C]ICI-OMe radioactivity (data not shown).

Ex vivo biodistribution in rat

Figure 5 shows radioactivity in plasma after *i.v.* injection of (*S*)-[^{11}C]ICI-OMe. There was a rapid loss of plasma radioactivity during the first 5 min after radiotracer injection, followed by a slow clearance. Predosing animals by *i.v.* injection of β-antagonists had no effect on the clearance of radioactivity.

Figure 6 illustrates uptake of radioactivity in various tissues as a function of time after injection of (*S*)-[^{11}C]ICI-OMe given 5 min after vehicle (ethanol/saline, 1/1, v/v), unlabelled (*S*)-ICI-OMe, propranolol or CGP 20712A. In all tissues, maximum radioactivity was observed at the first dissection time (1 min). After the initial peaks, radioactivity cleared more slowly from tissues than from plasma consistent with a small uptake in extravascular compartments. Predosing with unlabelled (*S*)-ICI-OMe, propranolol or CGP 20712 had a small effect on clearance from myocardium and lung. Radioactivity was detected in the urine at all times after injection of tracer (data not shown).

One experiment (6 rats) was carried out to investigate the effect of predosing with the β_1-AR selective antagonist CGP 20712A compared with that of the non-selective antagonist CGP 12177. Figure 7 shows the results combined with data from other predosing studies (Fig. 6, 20 min). A high dose of CGP 20712A (5 μmol·kg^{-1}) had a small effect on myocardial uptake of (*S*)-[^{11}C]ICI-OMe radioactivity whereas lower doses had even less (100 nmol·kg^{-1}) or no (10 nmol·kg^{-1}) effect. CGP 20712A had little effect on lung radioactivity. CGP12177 (5 μmol·kg^{-1}), however, had no effect on (*S*)-[^{11}C]ICI-OMe radioactivity in myocardium but reduced that in lung. Propranolol at high dose (5 μmol·kg^{-1}) had a small effect on both myocardial and lung radioactivity.

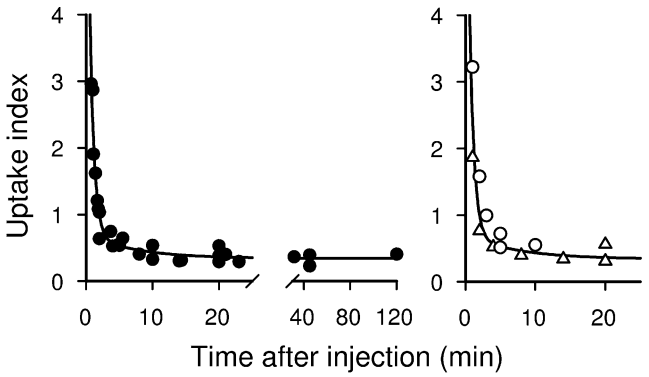

Fig. 5 Clearance of radioactivity from plasma of rats after *i.v* injection of (*S*)-[^{11}C]ICI-OMe. (*S*)-[^{11}C]ICI-OMe (3–7 MBq·kg^{-1}, undetectable-2.2 nmol·kg^{-1}) was given 5 min after vehicle (ethanol/saline, 1/1, v/v) (•), unlabelled (*S*)-ICI-OMe at 2 μm·kg^{-1} (○) or propranolol at 5 μmol·kg^{-1}(Δ). 1–6 serial blood samples were taken from each rat. Lines are the bi-exponential fit for radioactivity versus time for vehicle and (*S*)-[^{11}C]ICI-OMe

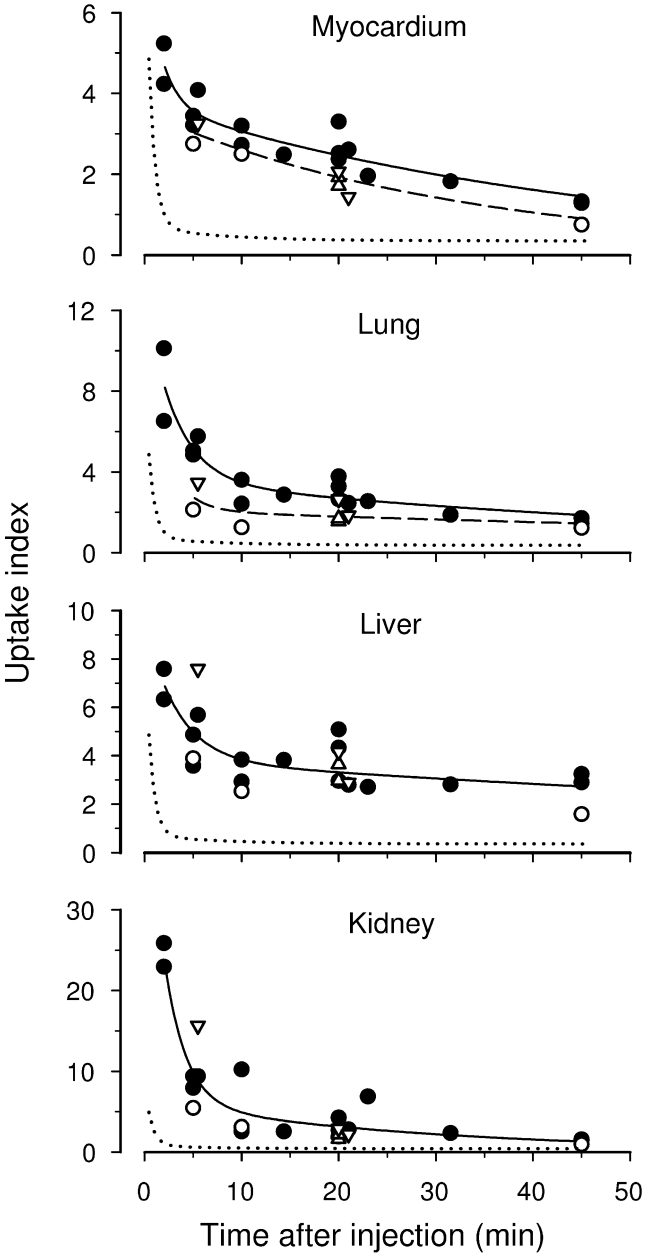

Fig. 6 Radioactivity in tissues of rats after *i.v* injection of (*S*)-[^{11}C]ICI-OMe. Each symbol indicates an uptake index for one rat. (*S*)-[^{11}C]ICI-OMe (0.5–7 MBq·kg^{-1}, undetectable-2.2 nmol·kg^{-1}) was given 5 min after vehicle (ethanol/saline, 1/1, v/v) (•), unlabelled (*S*)-ICI-OMe at 2 μm·kg^{-1} (○), propranolol at 5 μmol·kg^{-1} (Δ) or CGP 20712A at 5 μmol·kg^{-1} (▽). The solid lines are fitted to data for (*S*)-[^{11}C]ICI-OMe radioactivity after vehicle and the broken lines to data after unlabelled (*S*)-ICI-OM, propranolol and CGP 20712A. Dotted lines show the fit to data for plasma from Fig. 5

Radioactive metabolites

Figure 8 shows HPLC analysis of tissue samples taken at 5 min after *i.v.* injection of (*S*)-[^{11}C]ICI-OMe. Chromatograms for plasma and liver demonstrated (*S*)-[^{11}C]ICI-OMe (elution time 20–25 min) and polar metabolites. In plasma, two radioactive peaks were detected near the solvent front (1.5–2.5 min and 2.9–3.7 min) whereas in liver radioactive metabolites eluted at 19–20 min. Analysis of both myocardium and urine revealed one major radioactive peak at 20–23 min corresponding to (*S*)-[^{11}C]ICI-OMe.

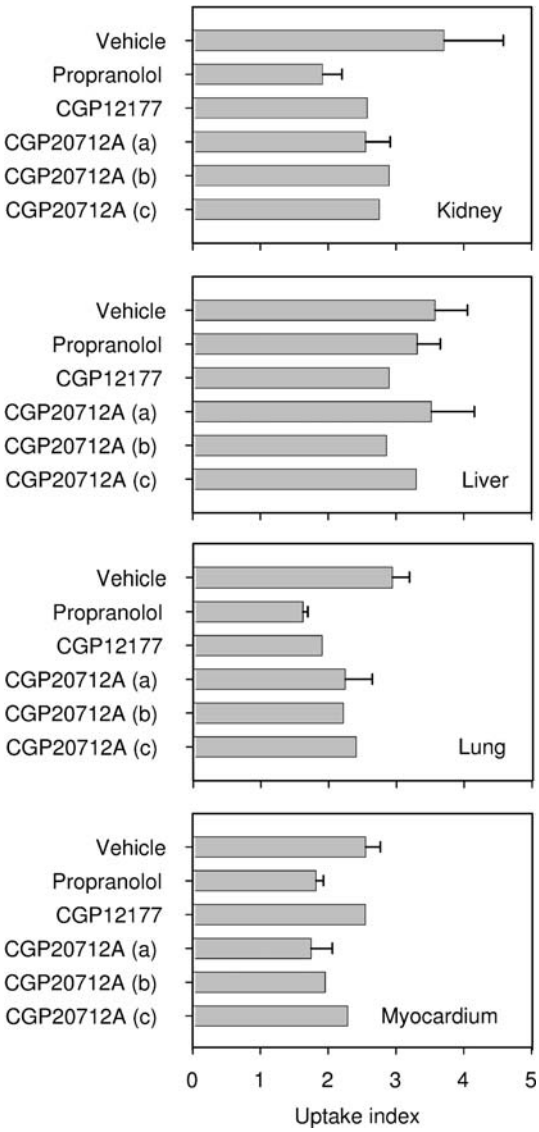

Fig. 7 Biodistribution of radioactivity in tissues of rats 20 min after *i.v* injection of (*S*)-[^{11}C]ICI-OMe (3–7 MBq·kg^{-1}, undectable-2.2 nmol·kg^{-1}). Bars indicate average values for uptake indices and standard errors or ranges are shown. (*S*)-[^{11}C]ICI-OMe was given 5 min after vehicle (ethanol/saline, 1/1, v/v) (5 rats), propranolol at 5 μmol·kg^{-1} (2 rats), CGP 12177 at 5 μmol·kg^{-1} (1 rat) or CGP 20712A at 5 μmol·kg^{-1} (*a*, 2 rats), 100 nmol·kg^{-1} (*b*, 1 rat) or 10 nmol·kg^{-1} (*c*, 1 rat)

Different HPLC profiles were observed for samples taken at other times after *i.v.* injection. Both (*S*)-[^{11}C]ICI-OMe and polar metabolites were observed in plasma at 2 min after injection but at 15 and 20 min only the more polar metabolite was seen. In liver at 15 min, there was one

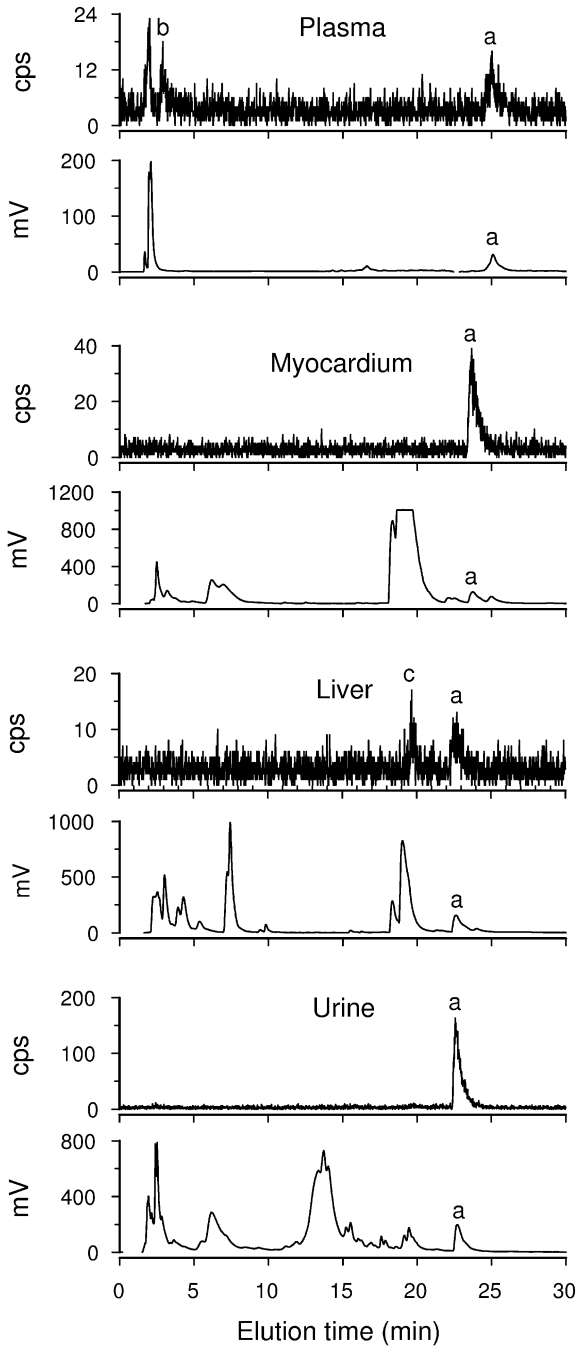

Fig. 8 HPLC traces for samples of plasma, myocardium, liver and urine taken 5 min after *i.v.* injection of (*S*)-[^{11}C]ICI-OMe into a rat (60 MBq to a 294 g rat, 23 nmol·kg^{-1}). Each sample was spiked with unlabelled (*S*)-ICI-OMe to identify its elution time for each individual analysis. In each panel the upper trace shows radioactivity (cps) and the lower UV absorbance (mV). (*S*)-[^{11}C]ICI-OMe (*a*) and radioactive metabolites (*b*, *c*) were identified in plasma and liver but only (*S*)-[^{11}C]ICI-OMe (a) was detected in myocardium and urine

metabolite but no (*S*)-[^{11}C]ICI-OMe. In heart and urine at 15 min, however, only parent (*S*)-[^{11}C]ICI-OMe was detected.

[^{11}C]CO_2 in exhaled air and plasma

Radioactivity, presumably due to [^{11}C]CO_2, was detected in exhaled air during the first minute after *i.v.* injection of (*S*)-[^{11}C]ICI-OMe (Fig. 9). Exhaled radioactivity reached a maximum within 5 min. Integrating the area under the time activity curves indicated that only a small percentage (2–3%) of the injected radioactivity was trapped. The radioactivity in the second 70 ml NaOH trap, measured at the end of the study (after 4–5 half lives after injection of radioactivity but decay corrected), was < 1% of the total collected in the small traps.

[^{11}C]CO_2 was also detected in blood during the first minute after *i.v.* injection of (*S*)-[^{11}C]ICI-OMe (Fig. 9). This percentage of total radioactivity due to [^{11}C]CO_2 reached a maximum at 15–20 min and subsequently decreased to a stable level.

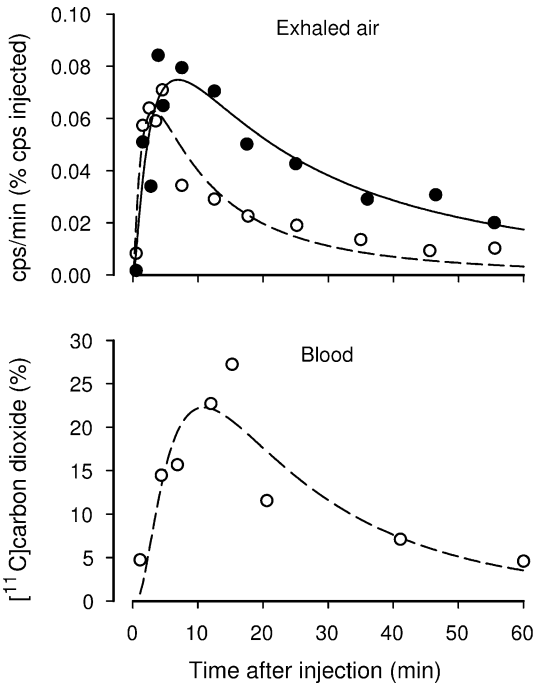

Fig. 9 [^{11}C]CO_2 in exhaled air and plasma. Two anaesthetised rats were injected with (*S*)-[^{11}C]ICI-OMe (10 MBq, 30 nmol·kg^{-1}) and their exhaled air drawn through NaOH (8 ml in 10 ml vials), using a vacuum pump, to trap radioactivity due to [^{11}C]CO_2. (● rat 1; ○ rat 2). Radioactivity in each vial, expressed as cpm/min (%)=100*(cpm in vial/collection time in minutes)/(cpm injected into rat), is plotted against mid-collection time (upper panel). Blood samples were taken from rat 2 and the percentage of radioactivity in blood due to [^{11}C]CO_2 was assessed (lower panel)

Discussion

The heart was clearly visible in quadHIDAC scans of rats following *i.v.* injection of (*S*)-[^{11}C]ICI-OMe (Fig. 3). Myocardial uptake of radioactivity, however, was low. Regions of interest drawn in the left ventricular wall typically gave average values of 170 cps·ml^{-1} at 5–15 min after injection of 8 MBq (*S*)-[^{11}C]ICI-OMe, and 150 cps·ml^{-1} after 8 MBq [^{18}F]FDG. There was uptake of radioactivity in liver, kidney and bladder.

After vascular mixing following injection of (*S*)-[^{11}C]ICI-OMe (0–30 s), there was a rapid loss of 'radioactivity' (coincident events per second) from myocardium (Fig. 4). Ex vivo dissection studies showed that plasma radioactivity decreased to ~10% during the first 5 min after injection of (*S*)-[^{11}C]ICI-OMe (Fig. 5). The apparent loss of myocardial radioactivity observed during 0.5 to 5 min (Fig. 4), therefore, is due to a combination of decreases in radioactivity in the myocardial microcirculation and of reduced spillover as radioactivity in the heart chambers decreases. Subsequently (> 5 min), there was a slow loss of myocardial radioactivity (Figs. 4, 6). HPLC analysis of tissue extracts (Fig. 8) showed that this radioactivity was due to unchanged (*S*)-[^{11}C]ICI-OMe. Injection of unlabelled (*S*)-ICI-OMe (2 μmol·kg^{-1}) (Fig. 4) or propranolol (5 μmol·kg^{-1}) (data not shown) at 15 min had no effect on the rate of loss of tracer radioactivity (Fig. 4) and predosing animals with unlabelled antagonists had no effect (Fig. 6).

To demonstrate specific binding of a radioligand to a receptor by predosing or displacement using unlabelled ligands, the amount of radioligand used should give low levels of receptor occupancy (< 1%) [33]. For high affinity ligands, it may not be possible to achieve the specific activity required to allow the injection of sufficient radioactivity to acquire statistically significant PET data while maintaining low receptor occupancy in small animals. In other words, if the radioactivity required for PET is equivalent to a ligand dose which saturates the receptor of interest, it will not be possible to demonstrate specific receptor binding using PET.

The doses of (*S*)-[^{11}C]ICI-OMe used in the PET studies ranged from 1–5 nmol·kg^{-1}. For the non-selective β-AR ligand (*S*)-[^{11}C]CGP 12177 injected intravenously into rats, a dose of 1.3 nmol·kg^{-1} halved myocardial uptake of radioactivity and 15 nmol·kg^{-1} completely blocked it [34]. In vitro membrane binding studies show that the K_D for CGP 12177 is 0.19–0.67 nM [35–39] as compared to the K_i value of 0.07 nM observed for (*S*)-ICI-OMe [28]. In other words, the affinity of (*S*)-ICI-OMe to β_1-AR in vitro is 3–10 times greater than that for (*S*)-CGP 12177 to β-AR. Using current [^{11}C]labelling methods, unlabelled *S*-ICI-OMe is synthesised with (*S*)-[^{11}C]ICI-OMe. It is feasible, therefore, that the 1–5 nmol·kg^{-1} used in the PET scans

gives an in vivo occupancy by unlabelled *S*-ICI-OMe which is too high for the detection of specific binding of (*S*)-[^{11}C]ICI-OMe to β_1-AR by predosing or displacement experiments.

The ex vivo biodistribution studies, however, failed to demonstrate high specific binding although the doses of (*S*)-[^{11}C]ICI-OMe ranged from undetectable (< 0.003 nmol·kg^{-1}) to 2 nmol·kg^{-1}. Predosing with high dose (*S*)-ICI-OMe (5 μmol·kg^{-1}) had little effect on myocardial radioactivity (Fig. 6). The selective β_1-AR antagonist CGP 20712A at high dose (5 μmol·kg^{-1}) had a small blocking effect but lower doses had even less (100 nmol mol·kg^{-1}) or no (10 n mol·kg^{-1}) effect (Fig. 7), suggesting that the half saturation dose for CGP 29712A for myocardium in vivo is between 10 nmol·kg^{-1} and 100 nmol·kg^{-1}. Comparable in vivo experiments have shown that the half saturation dose for CGP 12177 was ~1 nmol·kg^{-1} for rat myocardium [34]. Interestingly, one in vitro binding study in equine myocardium has shown a K_i for CGP 20712A of 30 nM, assessed against [^{3}H]CGP 12177, compared with a K_d for [^{3}H]CGP 12177 of 0.5 nM [51].

HPLC studies showed that myocardial radioactivity represented parent (*S*)-[^{11}C]ICI-OMe [Fig. 8]. The very small effect of unlabelled selective β-AR antagonists coupled with the clearance of radioactivity from the myocardium, however, suggests that (*S*)-[^{11}C]ICI-OMe is bound predominantly to non-specific sites.

The metabolic studies show rapid breakdown of (*S*)-[^{11}C]ICI-OMe in other tissues (Fig. 8) and radioactivity was detected in exhaled air as early as the first minute after injection of radioligand (Fig. 9). Polar radiolabelled metabolites, eluting after the solvent front, were seen in plasma samples taken at 2–5 min after (*S*)-[^{11}C]ICI-OMe and a radiometabolite of intermediate polarity was found in liver (Fig. 8). These results are consistent with metabolism of (*S*)-[^{11}C]ICI-OMe to intermediates, which include radioactive methanol, in the liver. [^{11}C]Methanol is catabolised to [^{11}C]carbon dioxide via [^{11}C]formaldehyde and [^{11}C]formate [42–46]. The presence of parent (*S*)-[^{11}C]ICI-OMe in urine was unexpected. The absence of radiolabelled metabolites in urine, however, is consistent with metabolism of (*S*)-[^{11}C]ICI-OMe to [^{11}C]CO_2; under normal conditions bicarbonate is effectively reabsorbed by kidney tubules.

Rapid metabolism of (*S*)-[^{11}C]ICI-OMe in liver and, possibly, lung could result in a low availability of radioligands to myocytes and consequently a very low occupancy of myocardial β_1-AR. Other radiolabelled analogues of ICI 89,406 may be less susceptable to metabolism. We have recently synthesised the fluorinated analogues (*R*)- and (*S*)-*N*-[2-[3-(2-cyano-phenoxy)-2-hydroxy-propylamino]-ethyl]-*N*′-[4-(2-fluoro-ethoxy)-phenyl]-urea [52]. In vitro studies showed that the (*S*)-enantiomer had higher β_1-AR selectivity and affinity than the (*R*)-enantiomer (affinity K_{i1}=0.049 nM vs K_{i1}=0.297 nM; selectivity 40800 *vs* 1580). The [^{18}F]-labelled (*S*)-analogue was synthesised at a higher specific activity (40 GBq·μmol^{-1} at EOS) than was achieved for (*S*)-ICI-OMe (6.5 GBq·μmol^{-1} at EOS). This result, coupled with the other advantages of ^{18}F compared with ^{11}C for PET imaging (e.g. better image resolution, half life 110 min *vs* 20 min) has encouraged us to begin in vivo evaluation of this compound.

Conclusion

The *O-methyl* derivative of the β_1-adrenoceptor antagonist ICI 89,406 was labelled with carbon-11 ((*S*)-[^{11}C]ICI-OMe). Although in vitro membrane studies showed that (*S*)-ICI-OMe has high affinity and selectivty for β_1-ARs, the present study in rats failed to demonstrate the high specific binding of (*S*)-[^{11}C]ICI-OMe to myocardial β_1-AR following intravenous injection which is a prerequisite for use in PET. A new [^{18}F-labelled derivative of ICI 89,406 has been synthesised and is under evaluation.

Acknowledgements This work was supported by grants from the Deutsche Forschungsgemeinschaft (DFG), Sonderforschungsbereich 656 MoBil Münster, Germany (project A1, A5), by the Interdisciplinary Clinical Research Centre, Münster (IZKF, project ZPG 4b), Germany, and by the EC - FP6-project DiMI (WP 11.1), LSHB-CT-2005-512146). Dr. V.W. Pike is supported by the Intramural Research Program of the National Institutes of Health (the National Institute of Mental Health), USA. The authors would like to thank Dr. Klaus Schäfers for advice on HIDAC scanning and for software for image analysis and Ms Christine Bätza, Ms Irmgard Hoppe and Ms Sandra Schröer for technical assistance.

References

1. Molenaar P, Parsonage WA. Fundamental considerations of β-adrenoceptor subtypes in human heart failure. Trends Pharmacol Sci 2005;26:368–75.
2. Brodde O-E, Bruck H, Leineweber K. Cardiac adrenoceptors: physiological and pathophysiological relevance. J Pharmacol Sci 2006;100:323–37.
3. Lohse MJ, Engelhardt S, Eschenhagen T. What is the role of β-adrenergic signaling in heart failure? Circ Res 2003;93:896–06.
4. Bristow MR, Ginsburg R, Umans V, Fowler M, Minobe W, Rasmussen R, et al. β_1- and β_2- adrenergic-receptor subpopulations in nonfailing and failing human ventricular myocardium: coupling of both receptor subtypes to muscle contraction and selective β_1-receptor down-regulation in heart failure. Circ Res 1986;59:297–309.
5. Khamssi M, Brodde O-E. The role of cardiac β_1- and β_2-adrenoceptor stimulation in heart failure. J Cardiovasc Pharmacol 1990;16 Suppl 5:S133–7.
6. Steinfath M, Geertz B, Schmitz W, Scholz H, Haverich A, Breil I, et al. Distinct downregulation of cardiac β_1 and β_2 adrenoceptors in different human heart diseases. Naunyn-Schmiedeberg's Arch Pharmacol 1991;343:217–20.

7. Steinfath M, Lavicky J, Schmitz W, Scholz H, Döring V, Kalmár P. Regional distribution of β_1- and β_2-adrenoceptors in the failing and nonfailing human heart. Eur J Clin Pharmacol 1992;42:607–11.
8. Steinfath M, Lavicky J, Schmitz W, Scholz H, Döring V, Kalmar P. Changes in cardiac β-adrenoceptors in human heart diseases: relationship to the degree of heart failure and further evidence for etiology-related regulation of β_1 and β_2 subtypes. J Cardiothorac Vasc Anesth 1993;7:668–73.
9. Brodde O-E, Zerkowski HR, Doetsch N, Motomura S, Khamssi M, Michel MC. Myocardial β-adrenoceptor changes in heart failure: concomitant reduction in β_1- and β_2-adrenoceptor function related to the degree of heart failure in patients with mitral valve disease. J Am Coll Cardiol 1989;14:323–31.
10. Leineweber k, Büscher R, Bruck H, Brodde O-E. β-adrenoceptor polymorphisms. Naunyn-Schmiedeberg's Arch Pharmacol 2004;369:1–22.
11. Delforge J, Syrota A, Lancon JP, Nakajima K, Loc'h C, Janier M, et al. Cardiac β-adrenergic receptor density measured in vivo using PET, CGP 12177, and a new graphical method. Nucl Med 1991;32:739–48.
12. Schäfers M, Dutka D, Rhodes CG, Lammertsma AA, Hermansen F, Schober O, et al. Myocardial presynaptic and postsynaptic autonomic dysfunction in hypertrophic cardiomyopathy. Circ Res 1998;82:57–62.
13. Schäfers M, Lerch H, Wichter T, Rhodes CG, Lammertsma AA, Borggrefe M, et al. Cardiac sympathetic innervation in patients with idiopathic right ventricular outflow tract tachycardia. J Am Coll Cardiol 1998;32:181–6.
14. Wichter T, Schäfers M, Rhodes CG, Borggrefe M, Lerch H, Lammertsma AA, et al. Abnormalities of cardiac sympathetic innervation in arrhythmogenic right ventricular cardiomyopathy: quantitative assessment of presynaptic norepinephrine reuptake and postsynaptic β-adrenergic receptor density with positron emission tomography. Circulation 2000;101:1552–8.
15. Kies P, Wichter T, Schäfers M, Paul M, Schäfers KP, Eckardt L, et al. Abnormal myocardial presynaptic norepinephrine recycling in patients with the Brugada syndrome. Circulation 2004;110:3017–22.
16. de Jong RM, Willemsen ATM, Slart RHJA, Blanksma PK, van Waarde A, Cornel JH, et al. Myocardial β-adrenoceptor down-regulation in idiopathic dilated cardiomayopathy measured in vivo with PET using the new radioligand (*S*)-[^{11}C]CGP12388. Eur J Nucl Med Mol Imaging 2005;32:443–7.
17. van Waarde A, Maas B, Doze P, Slart RH, Frijlink HW, Vaalburg W, et al. Positron emission tomography studies of human airways using an inhaled β-adrenoceptor antagonist, S-^{11}C-CGP 12388. Chest 2005;128:3020–7.
18. Valette H, Dolle F, Guenther I, Demphel S, Rasetti C, Hinnen F, et al. Preliminary evaluation of 2-[4-[3-tert-butylamino)-2-hydroxypropoxy]phenyl]-3-methyl-6-methoxy-4(3H)-quinazolinone ([+/−]HX-CH 44) as a selective β_1-adrenoceptor ligand for PET. Nucl Med Biol 1999;26:105–9.
19. Soloviev DV, Matarrese M, Moresco RM, Todde S, Buonasera TA, Sudati F, et al. Asymmetric synthesis and preliminary evaluation of (*R*)- and (*S*)-[^{11}C]bisoprolol, a putative β_1-selective adrenoceptor radioligand. Neurochem Int 2001;38:169–80.
20. Elsinga PH, van Waarde A, Visser GM, Vaalburg W. Synthesis and preliminary evaluation of (R,S)-1-[2-((carbamoyl-4-hydroxy) phenoxy)-ethylamino]-3-[4-(1-[^{11}C]-methyl-4-trifluoromethyl-2-imidazolyl)phenoxy]-2-propanol ([^{11}C]CGP 20712A) as a selective β_1-adrenoceptor ligand for PET. Nucl Med Biol 1994; 21:207–11.
21. van Waarde A, Meeder JG, Blanksma PK, Bouwer J, Visser GM, Elsinga PH, et al. Suitability of CGP-12177 and CGP-26505 for quantitative imaging of β-adrenoceptors. Int J Appl Instrum B 1992;19:711–8.
22. Imperial Chemical Industries Limited, London (UK), Patent CH 605666 1978; DE 2458908 1975. Chem Abstr 1976;84:43599.
23. Majid PA, Schreuder JE, de Feyter PJ, Roos JP. Clinical, electrocardiographic, and hemodynamic effects of ICI 89,406, a new cardioselective β-adrenoceptor antagonist with intrinsic sympathomimetic activity, in patients with angina pectoris. J Cardiovasc Pharmacol 1980;2:435–44.
24. Svendsen TL, Hartling O, Trap-Jensen J. Immediate haemodynamic effects of propranolol, practolol, pindolol, atenolol and ICI 89,406 in healthy volunteers. Eur J Clin Pharmacol 1979; 15:223–8.
25. Kopka K, Wagner S, Riemann B, Law MP, Puke C, Luthra SK, et al. Design of new β_1-selective adrenoceptor ligands as potential radioligands for in vivo imaging. Bioorg Med Chem 2003;11: 3513–27.
26. Riemann B, Law MP, Kopka K, Wagner S, Luthra SK, Pike VW, et al. High non-specific binding of the β_1-selective radioligand 2-[^{125}I]-ICI-H. Nuklearmedizin 2003;42:173–80.
27. Wagner S, Kopka K, Law MP, Riemann B, Pike VW, Schober O, et al. Synthesis and first in vivo evaluation of new selective high affinity -adrenoceptor radioligands for SPECT based on ICI 89,406. Bioorg Med Chem 2004;12:4117–32.
28. Wagner S, Law MP, Riemann B, Pike VW, Breyholz H-J, Höltke C, et al. Synthesis of (*R*)- and (*S*)-[O-*methyl*-^{11}C]*N*-[2-[3-(2-cyanophenoxy)-2-hydroxy-propylamino]-ethyl]-*N*′-(4-methoxy-phenyl)-urea as candidate high affinity β_1-adrenoceptor PET radioligands. J Label Compd Radiopharm 2005;48:721–33.
29. Jeavons AP, Chandler RA, Deuttman CAR. A 3D HIDAC-PET camera with sub-millimeter resolution for imaging small animals. IEEE Trans Nucl Sci 1999;3:468–73.
30. Schäfers KP, Reader AJ, Kriens M, Knoess C, Schober O, Schäfers M. Performance Evaluation of the 32-module quadHIDAC small animal PET scanner. J Nucl Med 2005;46:996–1004.
31. Missimer J, Madi Z, Honer M, Keller C, Schubiger A, Ametamey SM. Performance evaluation of the 16-module quad-HIDAC small animal PET camera. Phys Med Biol 2004;49:2069–81.
32. Kopka K, Law MP, Breyholz H-J, Höltke C, Faust A, Riemann B, et al. Non-invasive molecular imaging of β-adrenoceptors in vivo: perspectives for PET-radioligands. Curr Med Chem 2005;12: 2057–74.
33. Hume SP, Gunn RN, Jones T. Pharmacological constraints associated with positron emission tomographic scanning of small laboratory animals. Eur J Nucl Med 1988;25:173–6.
34. Law MP. Demonstration of the suitability of CGP 12177 for in vivo studies of β-adrenoceptors. Brit J Pharmacol 1993;109: 1101–9.
35. Nanoff C, Freissmuth M, Schütz W. The role of a low β_1-adrenoceptor selectivity of [^{3}H]CGP-12177 for resolving subtype-selectivity of competitive ligands. Naunyn-Schmiedeberg's Arch Pharmacol 1987;336:519–25.
36. Lin CH, Yang CM, Chen CM, Ko FN, Teng CM. Pharmacological characteristics of BDTI, a new isoquinoline-derived β_2-adrenoceptor agonist, in canine trachea and rat heart. Pharmacology 1996;53:19–27.
37. Mysliveček J, Říčný J, Kolář F, Tuček S. The effects of hydrocortisone on rat heart muscarinic and adrenergic α_1, β_1 and β_2 receptors, propranolol-resistant binding sites and on some subsequent steps in intracellular signalling. Naunyn-Schmiedeberg´s Arch Pharmacol 2003;368:366–76
38. Mysliveček J, Nováková M, Palkovits M, Križanoyá O, Kvetňanský R. Distribution of mRNA and binding sites of adrenoceptors and muscarinic receptors in the rat heart. Life Sci 2006;79:112–20.

39. Horinouchi T, Morishima S, Tanaka T, Suzuki F, Tanaka Y, Koike K, et al. Pharmacological evaluation of plasma membrane β-adrenoceptors in rat hearts using the tissue segment binding method. Life Sc 2006;79:941–8.
40. Heubach JF, Trebeß I, Wettwer E, Himmel HM, Michel MC, Kaumann AJ, et al. L-type calcium current and contractility in ventricular myocytes from mice overexpressing the cardiac β_2-adrenoceptor. Cardiovasc Res 1999;42:173–82.
41. Kaumann AJ, Engelhardt S, Hein L, Molenaar P, Lohse M. Abolition of (−)-CGP 12177-evoked cardiostimulation in double β_1/β_2-adrenoceptor knockout mice. Obligatory role of β_1-adrenoceptors for putative β_4-adrenoceptor pharmacology. Naunyn-Schmiedeberg's Arch Pharmacol 2001;363:87–93.
42. Jacobsen D, McMartin KE. Antidotes for methanol and ethylene glycol poisoning. J Toxicol Clin Toxicol 1997;35:127–43.
43. Vale JA, Meredith TJ. Poisoning, Diagnosis and Treatment. London: Update Books; 1981.
44. Gosselin RE, Smith RP, Hodge HC. Clinical Toxicology of Commercial Products. 5th ed. Baltimore: Williams & Wilkins; 1984.
45. Jacobsen D, McMartin KE. Methanol and ethylene glycol poisonings. Mechanism of toxicity, clinical course, diagnosis and treatment. Med Toxicol 1986;1:309–34.
46. Eells JT, Black KA, Makar AB, Tedford CE, Tephly TR. The regulation of one-carbon oxidation in the rat by nitrous oxide and methionine. Arch Biochem Biophysics 1982;219:316–26.
47. Johlin FC, Fortman CS, Nghiem DD, Tephly TR. Studies on the role of folic acid and folate-dependent enzymes in human methanol poisoning. Mol Pharmacol 1987;31:557–61.
48. Reader AJ, Ally S, Bakatselos F, Manavaki R, Walledge RJ, Jeavons AP, et al. One-pass list-mode EM algorithm for high resolution 3D PET image reconstruction into large arrays. IEEE Trans Nucl Sci 2002;49:693–9.
49. Biedenstein S, Schafers M, Stegger L, Kuwert T, Schober O. Three-dimensional contour detection of left ventricular myocardium using elastic surfaces. Eur J Nucl Med 1999;26:201–7.
50. Gunn RN, Ranicar A, Yap JT, Wells P, Osman S, Jones T, Cunningham VJ. On-line measurement of exhaled [^{11}C]CO_2 during PET. J Nucl Med 2000;41:605–11.
51. Horn J, Bailey S, Berhane Y, Marr CM, Elliott J. Density and binding characteristics of β-adrenoceptors in the normal and failing equine myocardium. Equine Vet J 2002;34:406–11.
52. Wagner S, Law MP, Riemann B, Pike VW, Breyholz H-J, Höltke C, et al. Synthesis of an ^{18}F-labelled high affinity β_1-adrenoceptor PET radioligand based on ICI 89. J Label Compd Radiopharm 2006;49:177–95.